Article

Competition between Anion-Deficient Oxide and Oxyhydride Phases during the Topochemical Reduction of LaSrCoRuO$_6$

Zhilin Liang, Maria Batuk, Fabio Orlandi, Pascal Manuel, Joke Hadermann, and Michael A. Hayward*

Read Online

ACCESS | Metrics & More | Article Recommendations | Supporting Information

ABSTRACT: Binary metal hydrides can act as low-temperature reducing agents for complex oxides in the solid state, facilitating the synthesis of anion-deficient oxide or oxyhydride phases. The reaction of LaSrCoRuO$_6$, with CaH$_2$ in a sealed tube yields the face-centered cubic phase LaSrCoRuO$_{3.2}$H$_{1.9}$. The reaction with LiH under similar conditions converts LaSrCoRuO$_6$ to a mixture of tetragonal LaSrCoRuO$_{4.8}$H$_{1.2}$ and cubic LaSrCoRuO$_{3.3}$H$_{2.13}$. The formation of the LaSrCoRuO$_x$H$_y$ oxyhydride phases proceeds directly from the parent oxide, with no evidence for anion-deficient LaSrCoRuO$_{6-x}$ intermediates, in contrast with many other topochemically synthesized transition-metal oxyhydrides. However, the reaction between LaSrCoRuO$_6$ and LiH under flowing argon yields a mixture of LaSrCoRuO$_5$ and the infinite layer phase LaSrCoRuO$_4$. The change to all-oxide products when reactions are performed under flowing argon is attributed to the lower hydrogen partial pressure under these conditions. The implications for the reaction mechanism of these topochemical transformations is discussed along with the role of the hydrogen partial pressure in oxyhydride synthesis. Magnetization measurements indicate the LaSrCoRuO$_x$H$_y$ phases exhibit local moments on Co and Ru centers, which are coupled antiferromagnetically. In contrast, LaSrCoRuO$_4$ exhibits ferromagnetic behavior with a Curie temperature above 350 K, which can be rationalized on the basis of superexchange coupling between the Co^{1+} and Ru^{2+} centers.
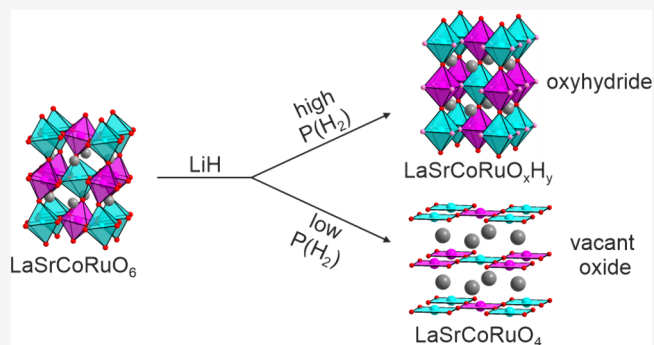
INTRODUCTION

The refractory nature of binary metal oxides means that the majority of complex transition-metal oxides are prepared at high temperature. These high-temperature "ceramic" synthesis reactions operate under thermodynamic control, resulting in the preparation of the most stable phase, or mixture of phases, for the particular chemical composition reacted. As a result, the range of complex transition-metal oxides, which can be prepared by these routes is quite limited, reflecting the limited number of oxidation states, metal coordination geometries, and three-dimensional packing schemes that are thermodynamically favored under these reaction conditions. Furthermore, there is limited scope to control the products that form for a particular composition, as it is hard to change the thermodynamic balance between product phases, with applied pressure and oxygen partial pressure typically the only parameters which can be used to exert some control.

Topochemical reactions—those that modify the composition of solid compounds by insertion, extraction, or exchange of species while retaining the original structural topology of the phase—can broaden the range of synthesizable solids significantly.[1] These reactions occur at low temperature, utilizing differences in the mobility of the constituent species in solids to bring about structure-conserving compositional changes. As a consequence, this class of reaction operates

under kinetic control, so the products are those phases that form fastest, rather than the phases that are the most thermodynamically stable, thus allowing the preparation of metastable solid compounds. Furthermore, as the identity of the products formed by this class of reaction depends on the relative rates of competing reactions, modification of these reaction rates offers a further way of controlling the products of synthesis in the solid-state.

Binary metal hydrides such as NaH, LiH, or CaH$_2$ are effective reagents for low-temperature topochemical anion extraction reactions.[1−3] For example, NaH can facilitate the topochemical reduction of LaNiO$_3$ to the Ni^{1+} phase LaNiO$_2$.[4] Likewise, CaH$_2$ can convert SrFeO$_{3-\delta}$ to SrFeO$_2$[5] and also be used to prepare a host of other anion-deficient complex oxides containing transition-metal cations in extremely low oxidation states such as Mn^{1+}, Co^{1+}, Ru^{2+}, or Ir^{2+}.[6−9]
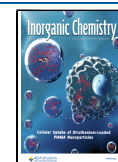
In addition, binary metal hydrides can also affect anion exchange reactions, allowing for the topochemical synthesis of oxyhydride compounds. Examples include the conversion of $LaSrCoO_4$ to $LaSrCoO_3H_{0.7}$[10] or the conversion of $LaSr_3NiRuO_8$ to $LaSr_3NiRuO_4H_4$,[11] facilitated by reaction with CaH_2 in both cases.

Here, we describe the reactivity of the double perovskite oxide, $LaSrCoRuO_6$, with binary metal hydrides (CaH_2, LiH) and observe a competition between anion-deficient oxide and oxyhydride product phases, which sheds light on the mechanism of the topochemical processes occurring.

■ EXPERIMENTAL SECTION

Synthesis of $LaSrCoRuO_6$. Samples of $LaSrCoRuO_6$ were prepared via a citrate gel method. Suitable stoichiometric ratios of La_2O_3 (99.999%), $SrCO_3$ (99.99%), Co powder (99.996%), and RuO_2 (99.99% dried at 800 °C) were dissolved in a minimum quantity of 6 M nitric acid. Three mol equiv of citric acid and 5 mL of analar ethylene glycol were added, and the solution was heated with constant stirring. The gels thus formed were subsequently ground into a fine powder, placed in an alumina crucible, and heated at 1 °C min^{-1} to 900 °C in air. The powders were then reground, pressed into 13 mm pellets, and then heated at 1100 °C in air for 2 periods of 24 h with intermediate regrinding. At the end of the final heating period, samples were cooled at a rate of 5 °C min^{-1} to 450 °C and then removed from the furnace, rapidly transferred to a dry ice-cooled alumina crucible, and allowed to rapidly cool. Synchrotron X-ray powder diffraction data collected from $LaSrCoRuO_6$ could be fit by a structural model previously reported for the phase (space group $P2_1/n$) to achieve a good fit as described in the Supporting Information.[12,13]

Topochemical Reduction of $LaSrCoRuO_6$. Samples of $LaSrCoRuO_6$ were reduced by the reaction with either LiH or CaH_2. Samples of $LaSrCoRuO_6$ were ground together with 4 mol equivalents of CaH_2 in an argon filled glovebox. The resulting mixtures were then sealed in evacuated Pyrex ampules and heated as described below. Alternatively, $LaSrCoRuO_6$ was ground together with 8 mol equivalents of LiH in an argon filled glovebox. These mixtures were either sealed in evacuated Pyrex ampules and subsequently heated as described below or poured into an open-ended Pyrex tube that was placed within a silica flow-tube, which could be sealed at each end with valves, so that the flow-tube assembly could be inserted into a clam-shell furnace while maintaining an argon atmosphere over the sample mixture. The flow-tube was then purged with argon for 20 min before being heated as described below, under a constant flow of argon, as shown schematically in Figure S8. Reaction progress was monitored by X-ray powder diffraction.

After reaction, samples reduced using LiH were washed with methanol under a nitrogen atmosphere to remove any unreacted LiH and Li_2O reaction by product. Samples reduced using CaH_2 were initially washed with a 0.1 M solution of NH_4Cl in methanol, under a nitrogen atmosphere, to remove any unreacted CaH_2 or CaO reaction byproduct before being washed with clean methanol.

Characterization. Reaction progress monitoring and initial structural characterization was performed using laboratory X-ray powder diffraction (PXRD) data collected using a PANalytical X'pert diffractometer incorporating an X'celerator position-sensitive detector (monochromatic Cu $K\alpha1$ radiation). Air-sensitive samples were measured in enclosed cells sealed under argon. High-resolution synchrotron powder X-ray diffraction (SXRD) data were collected using the I11 instrument at the Diamond Light Source Ltd. Diffraction patterns were collected by using Si-calibrated X-rays with an approximate wavelength of 0.825 Å from samples sealed in 0.3 mm diameter borosilicate glass capillaries.

Neutron powder diffraction (NPD) data were collected using the WISH diffractometer at the ISIS neutron source from samples contained within vanadium cans sealed under an inert atmosphere.

Rietveld refinement of powder diffraction data was performed using the TOPAS Academic software package (V6).[14]

Thermogravimetric analysis (TGA) measurements were performed by heating powder samples under flowing oxygen or nitrogen using a Mettler-Toledo MX1 thermogravimetric microbalance or a Perkin-nElmer microbalance with exhaust gases monitored by a Hiden Analytical Mass spectrometer. DC magnetization data were collected using a Quantum Design MPMS SQUID magnetometer from samples contained in gelatin capsules. Three-dimensional electron diffraction (3D ED) data were acquired with a FEI Titan 80−300 "cubed" microscope operated at 300 kV. The specimens for the TEM study were prepared by grinding the material in ethanol and depositing a few drops of the suspension onto a copper TEM grid covered by a continuous carbon layer. The specimens were prepared in an Ar-filled glovebox.

■ RESULTS

Topochemical Reactivity of $LaSrCoRuO_6$. $LaSrCoRuO_6$/CaH_2 mixtures were heated in sealed Pyrex ampules in the temperature range 330 < T/ °C < 380 for 8 day periods. No reaction was observed at temperatures below 350 °C. At temperatures greater than 370 °C, the $LaSrCoRuO_6$ perovskite phase decomposed to form mixtures of La_2O_3, SrO, Co, Ru, and CaO/CaH_2. However, in the range 350 < T/ °C < 370, PXRD data revealed a new cubic phase had formed (a = 7.67 Å), with reflection conditions consistent with the Fm-$3m$ (#225) space group. A sample for detailed analysis, henceforth referred to as "sample A", was prepared by heating ~1.5 g of $LaSrCoRuO_6$ with 4 mol equivalents of CaH_2 within sealed, cylindrical Pyrex ampules (internal diameter 10 mm, lengths 15−20 mm) at 360 °C for 3 periods of 8 days with intermediate regrinding, prior to washing to remove the calcium phases.

$LaSrCoRuO_6$/LiH mixtures were heated in sealed Pyrex ampules in the temperature range 300 < T/ °C < 340 for 8 day periods. No reaction was observed at temperatures below 310 °C. At temperatures greater than 330 °C, the $LaSrCoRuO_6$ perovskite phase decomposed. However, in the range 310 < T/ °C < 330, PXRD data revealed that a new, apparently tetragonal phase, had formed (a = 5.43 Å, c = 7.98 Å), with reflection conditions consistent with body-centering. A sample for detailed analysis, henceforth referred to as "sample B", was prepared by heating ~1.5 g of $LaSrCoRuO_6$ with 8 mol equivalents of LiH CaH_2 within sealed, cylindrical Pyrex ampules (internal diameter 10 mm, lengths 15−20 mm) at 320 °C for 3 periods of 8 days with intermediate regrinding, prior to washing to remove the lithium phases.

Analysis, detailed below, revealed that sample B is a mixture of $LaSrCoRuO_{6-x}H_y$ oxyhydride phases. To investigate the role of the H_2 partial pressure ($P(H_2)$) generated during the reaction, $LaSrCoRuO_6$/LiH mixtures were heated under flowing argon (to minimize the H_2 partial pressure) in the temperature range 300 < T/ °C < 390. No reaction was observed at temperatures below 335 °C, and sample decomposition was observed above 380 °C. However, in the temperature range 335 < T/°C < 360, PXRD data revealed the formation of two distinct phases, $LaSrCoRuO_5$ (prepared previously by reduction of $LaSrCoRuO_6$ with Zr)[15] and a tetragonal phase (a = 5.67 Å, c = 6.88 Å), which is identified as $LaSrCoRuO_4$, as described below. On raising the reaction temperature to 375 °C, $LaSrCoRuO_4$ became the majority phase, but it was not possible to prepare a single-phase sample of $LaSrCoRuO_4$ by this route, presumably due to the small oxygen partial pressure (~2−3 ppm) in the argon gas. In an

attempt to prepare a single-phase sample, the products from the reactions performed under flowing argon (which still contained some unreacted LiH) were sealed under vacuum in Pyrex ampules and heated at 375 °C for 24 h. PXRD data revealed that this led to the conversion of the LaSrCoRuO$_5$/ LaSrCoRuO$_4$ mixture to a mixture of LaSrCoRuO$_{6-x}$H$_y$ oxyhydride phases similar to those in sample B. Thus, a sample of "LaSrCoRuO$_4$" for detailed analysis, henceforth referred to as "sample C", was prepared by heating ~1.5 g of LaSrCoRuO$_6$ with 8 mol equivalents of LiH under flowing argon at 375 °C for 1 period of 2 days, prior to washing to remove the lithium phases.

Characterization of Sample A—LaSrCoRuO$_{3.2}$H$_{1.9}$. Thermogravimetric data collected while heating sample A under flowing oxygen (Figure S2) to oxidize it back to LaSrCoRuO$_6$ (confirmed by PXRD) reveal a mass gain of 9.27%, consistent with an initial composition of LaSrCoRuO$_{3.2}$. This is clearly an unrealistic composition, as it requires transition-metal oxidation states below +1, which we interpret as indicating the phase is an oxyhydride of the form LaSrCoRuO$_{3.2}$H$_y$. To determine the hydride content, iodometric titrations were performed to establish the transition-metal oxidation states, as described in detail in the Supporting Information, which indicated a composition of LaSrCoRuO$_{3.2}$H$_{1.9}$.

SXRD data collected from LaSrCoRuO$_{3.2}$H$_{1.9}$ could be indexed using a face-centered unit cell, with reflection conditions consistent with space group Fm-3m. Thus, a structural model was constructed based on a cubic double perovskite with an anion site occupancy of O$_{0.53}$H$_{0.32}$ (as determined from the iodometric titrations), and this was refined against the SXRD data. Close inspection revealed additional diffraction peaks attributed to a secondary SrO phase, so this was added to the model. A good fit to the data was achieved, as shown in Figure 1 and described in detail in Table 1.

Characterization of Sample B—LaSrCoRuO$_x$H$_y$. Thermogravimetric data collected while heating sample B under flowing oxygen (Figure S3) to oxidize it back to LaSrCoRuO$_6$ (confirmed by PXRD) reveals a mass gain of 5.86%, consistent with an initial composition of LaSrCoRuO$_{4.23}$. However, mass
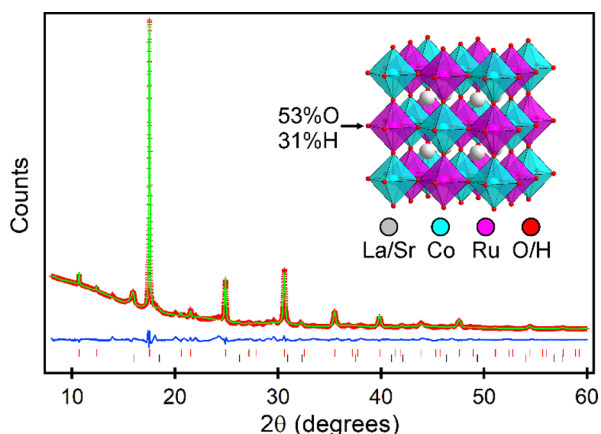

Figure 1. Observed calculated and difference plots from the structural refinement of LaSrCoRuO$_{3.2}$H$_{1.9}$ (sample A) against the SXRD data. Red tick marks indicate peak positions for the majority phase; black tick marks indicate a SrO secondary phase. The inset shows representation of the refined crystal structure.

Table 1. Parameters from the Structural Refinement of LaSrCoRuO$_{3.2}$H$_{1.9}$ (Sample A) against SXRD Data Collected at Room Temperature

atom	x	y	z	fraction	B_{iso} (Å^2)
La/Sr	1/4	1/4	1/4	0.5/0.5	3.05(4)
Co	0	0	0	1	2.82(5)
Ru	1/2	0	0	1	2.82(5)
O/H	1/2	0	1/4	0.53/0.32	3.18(3)

LaSrCoRuO$_{3.2}$H$_{1.9}$—space group Fm-3m (#225)

$a = 7.6679(1)$ Å, volume = 450.85(3) Å^3

formula weight = 439.64 g mol^{-1}, Z = 4

phase fraction = 96(1) mass %

SrO - space group Fm-3m (#225)

$a = 5.1465(5)$ Å, volume = 136.31(4) Å^3

formula weight = 103.62 g mol^{-1}, Z = 4

phase fraction = 4(1) mass %

radiation source: Synchrotron X-ray, λ = 0.8268 Å

temperature: 298 K

$R_p = 2.30\%$, $_wR_p = 3.34\%$, $R_{Bragg} = 1.03\%$

spectrometry measurements monitoring the exhaust gas of the TGA instrument at $m/z = 18$ (Figure S4) indicated a release of water coincident with the oxidation of the sample, indicating that the sample contained an oxyhydride phase.

SXRD and NPD data collected from sample B could only be indexed as two phases: a body-centered tetragonal phase (a = 5.43 Å, c = 7.98 Å) and a face-centered cubic phase (a = 7.71 Å). A structural model was constructed consisting of a cubic LaSrCoRuO$_{6-x}$ phase described in space group Fm-3m (#225) and a LaSrCoRuO$_{6-x}$ phase described in space group I4/m (#87). This 2-phase model was refined against the SXRD and NPD data, with the anion occupancies in the two phases allowed to refine freely. On convergence, the two-phase model had an average composition of LaSrCoRuO$_{3.28}$, significantly lower than the value determined from the TGA data (LaSrCoRuO$_{4.23}$). To address this, hydride ions were added to the model, such that each anion site could be occupied by either oxide ions, hydride ions, or be vacant. This model was refined with the constraints that the total sample oxygen content agreed with the TGA data and that the sum of the oxide and hydride occupancies on any anion site could not be greater than unity.

This model converged readily to yield compositions of LaSrCoRuO$_{4.80(1)}$H$_{1.20(1)}$ and LaSrCoRuO$_{3.30(6)}$H$_{2.13(9)}$ for the tetragonal and cubic phases, respectively. In addition, the tetragonal phase exhibits partial anion order with the 4e "axial" site fully occupied by oxygen, while the 8h "equatorial" site is a 0.7/0.3 mixture of oxygen and hydrogen as shown in Figure 2. This 2-phase model fits the SXRD data well as shown in Figure S6. However, close inspection of the NPD data (Figure 2) reveals a series of broad asymmetric peaks not indexed by the 2-phase model. Electron diffraction data (Figure S7) were collected to investigate the possibility that the broad features were due to short-range anion ordering. These data showed additional diffraction peaks indicating a doubling of the unit cell along the x- and y-axes of the tetragonal phase (ie. a $2\sqrt{2} \times 2\sqrt{2} \times 2$ expansion relative to the primitive perovskite unit cell). Such a cell expansion allows the broad asymmetric features in the NPD data to be indexed. However, it was not possible to construct a structural model in the expanded unit cell that accounts for the additional diffraction features while simultaneously fitting the sharp features in the data. This
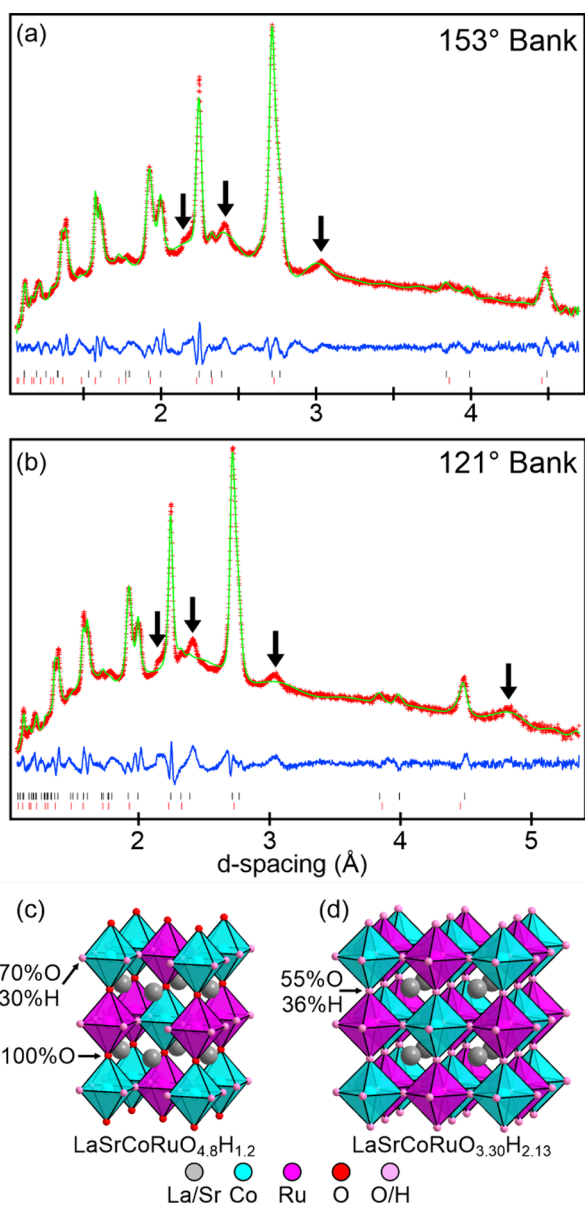
Figure 2. (a, b) Observed, calculated, and difference plots from the two-phase structural refinement of sample B against NPD data. Black tick marks indicate peak positions of LaSrCoRuO$_{4.8}$H$_{1.2}$, and red ticks indicate LaSrCoRuO$_{3.3}$H$_{2.13}$. Arrows indicate "supercell" reflections indicative of short-range anion order. Crystal structures of (c) LaSrCoRuO$_{4.8}$H$_{1.2}$ and (d) LaSrCoRuO$_{3.3}$H$_{2.13}$.

suggests that the anion order responsible for the expanded cell is short ranged and incomplete. A detailed description of the structural parameters of tetragonal LaSrCoRuO$_{4.80(1)}$H$_{1.20(1)}$ and cubic LaSrCoRuO$_{3.30(6)}$H$_{2.13(9)}$ are given in Table 2.

Characterization of Sample C—LaSrCoRuO$_4$. Thermogravimetric data collected while heating Sample C under flowing oxygen (Figure S9) to oxidize it back to LaSrCoRuO$_6$ (confirmed by PXRD) reveals a mass gain of 6.39%, consistent with an initial composition of LaSrCoRuO$_{4.07}$. NPD data collected from sample C could be indexed using a body-centered tetragonal unit cell (a = 5.67 Å, c = 6.88 Å) with a series of additional reflections attributable to the presence of small quantities of monoclinic LaSrCoRuO$_5$.[15] A 2-phase model was constructed combining a B-site ordered infinite

Table 2. Parameters from the 2-phase structural refinement of Sample B against NPD data collected at room temperature

			LaSrCoRuO$_{4.8}$H$_{1.2}$			
atom		x	y	z	fraction	B_{iso} (Å^2)
La/Sr	4d	0	$^1/_2$	$^1/_4$	0.5/0.5	0.46(14)
Co	2a	0	0	0	1	0.97(14)
Ru	2b	$^1/_2$	$^1/_2$	0	1	0.97(14)
O/ H(1)	8h	0.243(7)	0.257(8)	0	0.70(1)/ 0.30(1)	2.75(16)
O(2)	4e	0	0	$^1/_2$	1	2.75(16)

LaSrCoRuO$_{4.80(1)}$H$_{1.20(2)}$ − space group $I4/m$ (#87)
a = 5.4307(3) Å, c = 7.9842(8) Å, volume = 235.47(3) Å^3
formula weight = 464.54 g mol^{-1}, Z = 2
weight fraction= 65(1) mass %

		LaSrCoRuO$_{3.30}$H$_{2.13}$				
atom		x	y	z	fraction	B_{iso} (Å^2)
La/Sr	8c	$^1/_4$	$^1/_4$	$^1/_4$	0.5/0.5	0.46(14)
Co	4a	0	0	0	1	0.97(14)
Ru	4b	$^1/_2$	0	0	1	0.97(14)
O/H	24e	$^1/_2$	0	$^1/_4$	0.55(1)/0.36(2)	2.75(16)

LaSrCoRuO$_{3.30(6)}$H$_{2.13(9)}$ − space group Fm-$3m$ (#225)
a = 7.7154(7) Å, volume = 459.28(7) Å^3
formula weight = 441.48 g mol−1, Z = 4
weight fraction = 35(1) mass %
radiation source: neutron time-of-flight
temperature: 298 K
R_p = 1.37 %, $_wR_p$ = 1.88%

layer phase described in space group $I4/mmm$ and the reported structure of LaSrCoRuO$_5$.

This model was refined against the NPD data to achieve a good fit. To investigate the possibility of cooperative tilting of the MO$_4$ squares, a series of lower symmetry models were constructed. However, these lower symmetry models did not improve the fit to the data and were refined to give structures in which the Co−O−Ru bond angles remained 180°, within error, indicating the $I4/mmm$ model, detailed in Table 3, is the best description of the structure. The fit to the NPD data is shown in Figure 3.

Table 3. Parameters from the Structural Refinement of LaSrCoRuO$_4$ against NPD Data Collected at 300 K

atom	x	y	z	fraction	B_{iso}
La/Sr	0	$^1/_2$	$^1/_4$	0.5/0.5	0.24(4)
Co	0	0	0	1	1.94(6)
Ru	0	0	$^1/_2$	1	1.94(6)
O	0.2519(4)	0.2519(4)	0	1	1.97(5)

LaSrCoRuO4 − space group $I4/mmm$ (#139)
a = 5.6786(2) Å, c = 6.8823(4) Å, volume = 221.93(2) Å^3
formula weight = 450.53 g mol^{-1}, Z = 2
weight fraction = 91.7(3) %
LaSrCoRuO5 − space group $P112_1$ (#4)
a = 10.821(9) Å, b = 10.828(9) Å, c = 8.120(2) Å, γ = 91.02(3)°, volume = 951.2(1) Å^3
formula weight = 466.53 g mol^{-1}, Z = 8
weight fraction = 8.3(3) %
radiation source: neutron time-of-flight
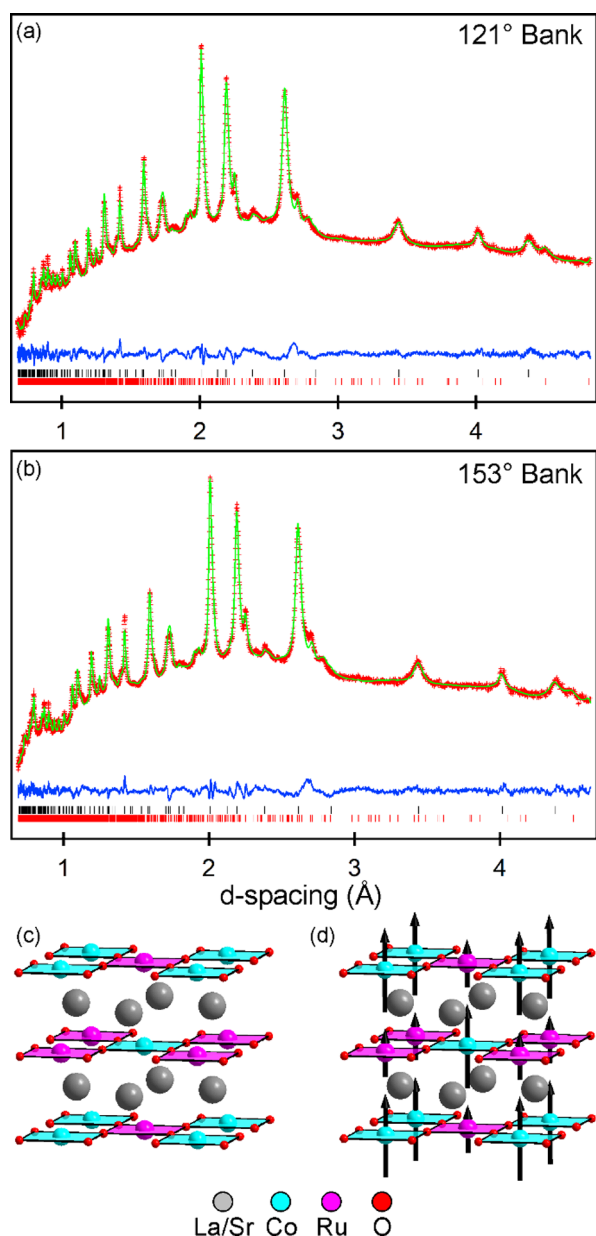temperature: 298 K
$_wR_p$ = 2.01%; Rp = 1.46%

Figure 3. (a, b) Observed, calculated and difference plots from the 2-phase structural refinement of Sample C against NPD data collected at 300 K. Black ticks indicate peak positions of LaSrCoRuO$_4$, red ticks LaSrCoRuO$_5$. (c) Crystal structure of LaSrCoRuO$_4$ at 300 K and (d) magnetic and crystal structure of LaSrCoRuO$_4$ at 5 K, ordered moments: Co 1.62 μB; Ru 0.21 μB.

Magnetic Characterization. Magnetization data collected from all reduced samples of LaSrCoRuO$_6$ contained signals from small quantities of ferromagnetic impurities (most likely elemental cobalt), in common with many other topochemically reduced phases. Thus, a "ferromagnetic subtraction" method was used to measure the magnetization of the samples, described in detail in the Supporting Information.

Magnetic susceptibility data collected in this manner from sample A (Figure 4a) could be fitted by the Curie–Weiss law in the range 150 < T/K < 300 (Figure S11, Supporting Information). However, the parameters extracted, C = 3.58(2) cm^3 K mol^{-1} and θ = −206(1) K, are much greater than those that can be accounted for by localized moments on the Co and Ru centers. The magnetization data exhibit a broad maximum

at T ≈ 50 K, suggestive of the onset of antiferromagnetic order, but given the level of chemical disorder in the anion lattice of sample A (LaSrCoRuO$_{3.2}$H$_{1.9}$), it is likely that any magnetic order present is short ranged.

Equivalent magnetic susceptibility data collected from sample B (Figure 4c) can also be fit by the Curie–Weiss law in the range 100 < T/K < 300 (Figure S12, Supporting Information). Again, the extracted parameters, C = 2.48(3) cm^3 K mol^{-1}, θ = 8.5(9) K, cannot easily be accounted for by local moments on the transition-metal centers. Below T = 100 K, the saturated moment of the sample (Figure 4d) exhibits a sharp rise, while the susceptibility reaches a local maximum at T ≈ 15 K, suggesting the onset of canted antiferromagnetic order. However, NPD data collected from sample B at 5 K show no indication of long-range magnetic order, suggesting any magnetic order present is short ranged in nature.

Magnetization data collected from sample C (LaSrCoRuO$_4$) are qualitatively different to data from the other phases. Magnetization-field isotherms collected from sample C at 300 K (Figure 5) indicate that the sample is ferromagnetic with a saturated moment of 0.45 μB per fu. Analogous data collected at 350 K (the highest temperature attainable in our apparatus) are also indicative of ferromagnetic behavior (saturated moment 0.2 μB per fu). Magnetization data collected from sample C as a function of temperature in the range 5 < T/K < 350 using the "ferromagnetic subtraction" technique (Figure S13) exhibit no obvious transition, suggesting the onset of ferromagnetic behavior is above 350 K, although the likely presence of ferromagnetic elemental Co impurities make this value of T_c less certain.

As noted above, NPD data collected from sample C at 300 K could be fitted without the need to include a magnetic model. However, NPD data collected at 5 K show a strong enhancement of the [110] and [101] reflections. These enhanced intensities are best fit using a magnetic model described in space group 139.537 (I4/mm'm') in which the moments on Co (1.62(6) μB) and Ru (0.21(7) μB) are aligned parallel to the z-axis, to yield a total ordered moment of 1.83(9) μB, in line with the saturated moment of 1.75 μB per fu extracted from the magnetization data. Full details of this structural refinement are given in the Supporting Information. Refinement of this magnetic model against the NPD data collected at 300 K yields ordered moments on Co and Ru that are smaller than the associated errors, indicating that while magnetization data indicate that LaSrCoRuO$_4$ is ferromagnetically ordered at 300 K, the magnetic scattering associated with this phase is not observable in the absence of an applied magnetic field.

DISCUSSION

Reactivity. The reactions that occur between binary metal hydrides (NaH, LiH, CaH$_2$) and complex transition-metal oxides yield products that can be organized into two main classes: (i) anion deficient oxide phases (ii) oxyhydride phases, which contain both O^{2-} and H$^-$ anions. Literature examples of the reactions that form these two product types are given in Scheme 1.[4,10,16,17]

The reactions in Scheme 1 show that the hydride ions in NaH act as 2-electron reducing agents in anion deintercalation reactions (NaH → NaOH),[4] while the hydride ions in LiH and CaH$_2$ act as 1-electron reducing agents (2LiH → Li$_2$O + H$_2$; CaH$_2$ → CaO + H$_2$)[10,16] with hydrogen gas produced during reactions which yield anion deficient oxide phases.
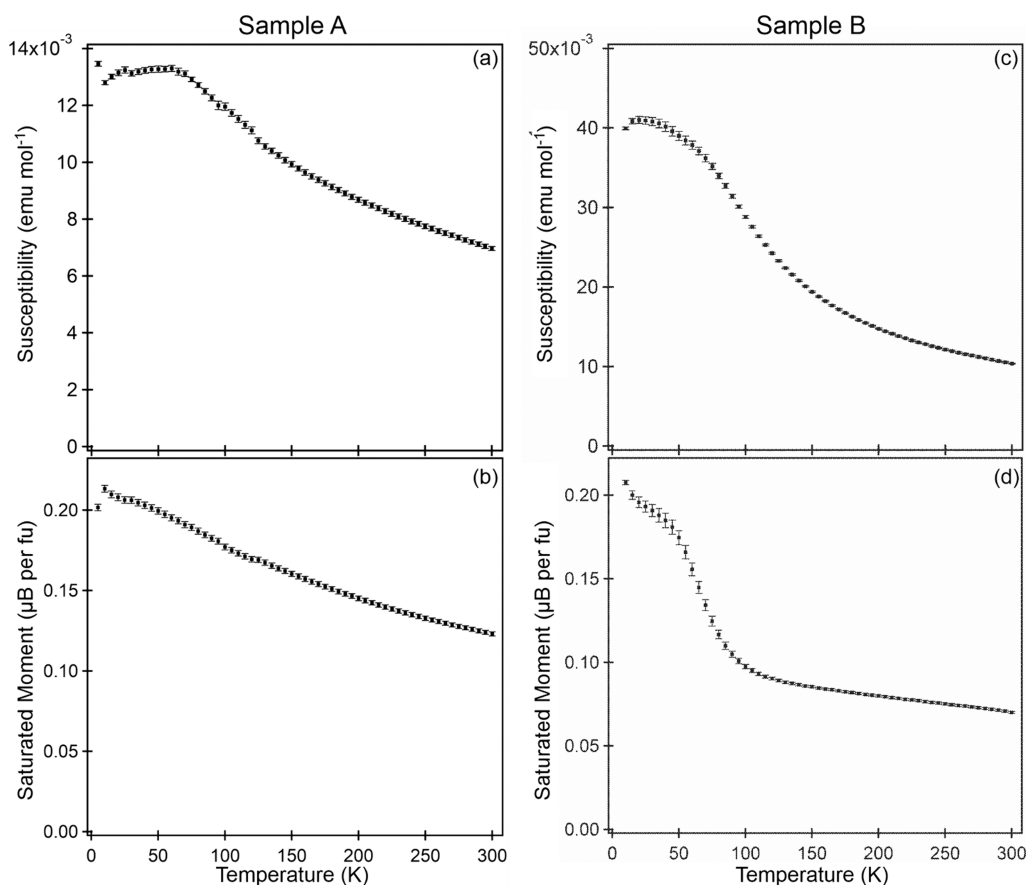
Figure 4. Magnetic susceptibility (a, c) and saturated ferromagnetic moment (b, d) data from sample A ($LaSrCoRuO_{3.2}H_{1.9}$) and sample B ($LaSrCoRuO_{4.8}H_{1.2}$ + $LaSrCoRuO_{3.30}H_{2.13}$), respectively.
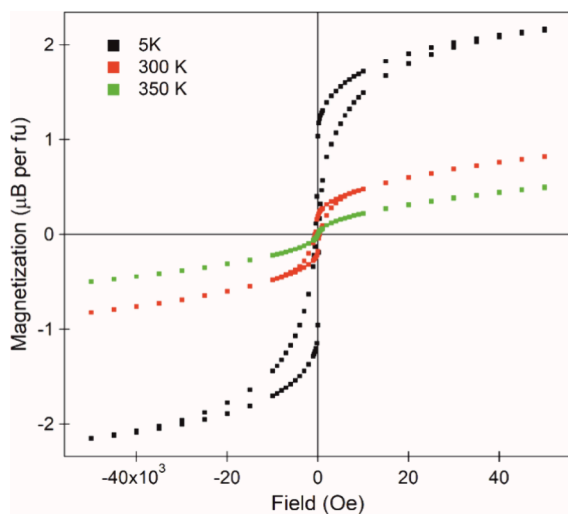
Figure 5. Magnetization-field data collected from sample C ($LaSrCoRuO_4$) at 350, 300, and 5 K.

Scheme 1. Reactions of Binary Hydrides with Complex Oxides

Anion Deintercalation

$$LaNiO_3 + NaH \rightarrow LaNiO_2 + NaOH$$

$$LaSrCoO_4 + 0.65CaH_2 \rightarrow LaSrCoO_{3.35} + 0.65CaO + 0.65H_2$$

$$Ba_{0.5}Sr_{0.5}MnO_3 + 2LiH \rightarrow Ba_{0.5}Sr_{0.5}MnO_2 + 2Li_2O + H_2$$

Oxyhydride Formation

$$LaSrCoO_{3.35} + 0.35CaH_2 \rightarrow LaSrCoO_3H_{0.7} + 0.35CaO$$

$$SrVO_3 + CaH_2 \rightarrow SrVO_2H + CaO + \tfrac{1}{2}H_2$$

Scheme 1 also shows that oxyhydride formation reactions are observed to occur either (a) via a simple redox-neutral anion exchange process as seen for $LaSrCoO_{3.35} \rightarrow LaSrCoO_3H_{0.7}$ with no generation of hydrogen,[10,18,19] or (b) as a combined reduction + anion-exchange reaction as observed for $SrVO_3 \rightarrow SrVO_2H$, with the generation of H_2 gas.[17]
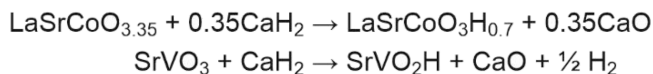
The redox-neutral anion-exchange process that forms oxyhydride compounds by route (a) starts with an anion-

deficient oxide phase, which is usually produced from an oxygen-stoichiometric compound by the action of the same binary hydride reagent that affects the hydride-for-oxide anion exchange (e.g., CaH_2). The result is a reaction sequence such as $LaSrCoO_4 \rightarrow LaSrCoO_{3.35} \rightarrow LaSrCoO_3H_{0.7}$, which only differs in total from the combined reduce + anion-exchange reactions in route (b) by the observation of an isolatable, anion-deficient all-oxide intermediate phase. Thus, the two observed topochemical routes for oxyhydride formation, (a) reduce-then-exchange or (b) reduce-and-exchange, can be considered as the extremes on a "spectrum" of oxyhydride formation reactions which differ only by how separate the "reduce" and "exchange" processes are.

In the context of the discussion above, the reactions between $LaSrCoRuO_6$ and the binary hydrides LiH and CaH_2 provide an interesting platform to study this type of chemistry. Figure 6
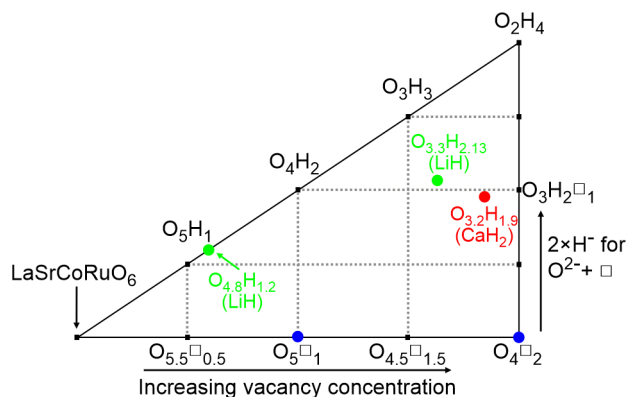

Figure 6. Phase diagram showing the topochemically reduced phases derived from $LaSrCoRuO_6$ via anion deintercalation and hydride-for-oxide anion exchange.

shows a phase diagram for the products of these topochemical reactions. Starting at stoichiometric $LaSrCoRuO_6$ on the left-hand side, moving horizontally across the diagram to the right corresponds to the reductive deintercalation of oxide ions to form $LaSrCoRuO_{6-x}$ phases. Thus, the two experimentally observed anion vacancy-ordered phases $LaSrCoRuO_5$ and $LaSrCoRuO_4$ are located on the bottom edge of the diagram (blue markers). Moving vertically up the diagram corresponds to the redox-neutral anion exchange of one O^{2-} oxide ion and one vacancy for two H^- hydride ions. Thus, the oxyhydride phases present in samples A (red marker) and B (green markers) lie away from the bottom axis. The phase diagram is bounded by a "top" edge, which corresponds to completely filling the anion sites with a combination of oxide and/or hydride ions, i.e., $LaSrCoRuO_xH_y$ phases where $x + y = 6$. It therefore follows that phases not located on the top edge of the diagram contain anion vacancies. It should also be noted that the diagram is arranged so that the oxidation states of the transition metals decline on moving to the right across the diagram.

The distribution of the five $LaSrCoRuO_{6-x}H_y$ phases experimentally isolated in this work show that unless efforts are made to actively lower the partial pressure of hydrogen (as was the case for sample C) reactions between $LaSrCoRuO_6$ and LiH or CaH_2 yield oxyhydride phases directly, with no evidence for the presence of anion-deficient all-oxide intermediates. This contrasts with the behavior of several previously studied cobalt oxide systems. For example, as noted above, $LaSrCoO_4$ reacts with CaH_2 at $T \approx 340\ °C$ to form $LaSrCoO_{3.35}$, which is then converted to $LaSrCoO_3H_{0.7}$ by further reaction with CaH_2 at $T > 450\ °C$ via the (a) reduce-then-exchange route.[10,18,19] Likewise, the Co/Ru phase $LaSr_3CoRuO_8$ is converted to $LaSr_3CoRuO_6$ on reaction with CaH_2 at 425 °C before further reaction at 450 °C yields $LaSr_3CoRuO_4H_4$.[20]

In the two examples described above, the reductive anion deintercalation step occurs at a lower temperature than the anion-exchange step. This indicates that the activation energy for the reductive step is lower than that of the anion-exchange step, as shown in the schematic energy diagram in Figure 7a. Thus, by supplying sufficient energy to overcome the first

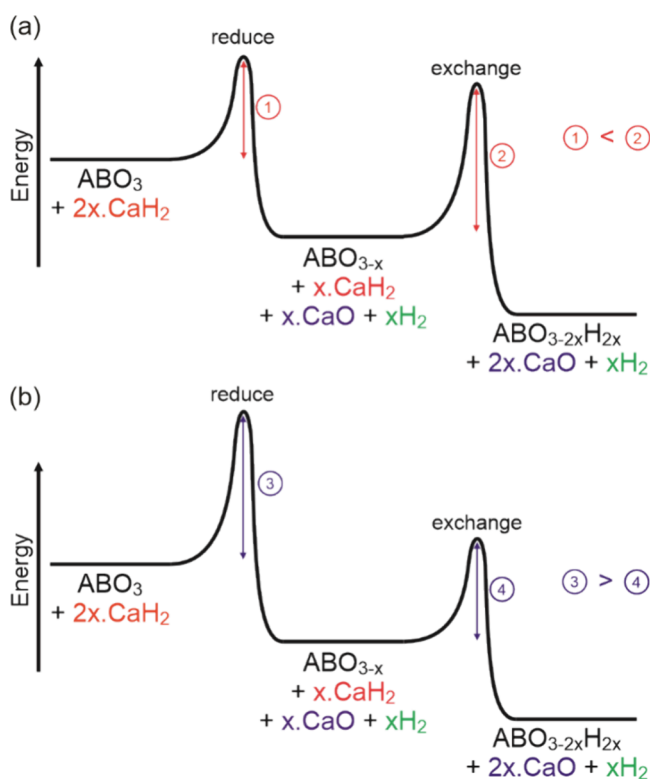barrier but not the second, an anion-deficient all-oxide phase can be isolated.

Figure 7. Schematic diagram showing the relative activation energies in the two classes of topochemical oxyhydride formation: (a) reduce-then-exchange and (b) reduce-and-exchange.

The direct conversion of $LaSrCoRuO_6$ to $LaSrCoRuO_{6-x}H_y$ oxyhydride phases, without any sign of anion-deficient all-oxide intermediates, indicates that, in this system, the activation energy for the anion-exchange step is equal to, or less than, the activation energy for the reductive deintercalation step, as shown in Figure 7b. As a result, as soon as sufficient energy is supplied to overcome the first barrier to form an anion deficient phase, there is enough energy to overcome the second barrier to convert it to an oxyhydride phase, so that no anion-deficient intermediate phase accumulates. This scenario of sequential reactions is supported by the observation that $LaSrCoRuO_{6-x}$ phases can be isolated from reactions between $LaSrCoRuO_6$ and LiH if the second reaction step (anion-exchange) is prevented, by keeping the $P(H_2)$ in the system low (i.e., performing the reaction under flowing argon), but that such "intermediates" will react rapidly with LiH to yield $LaSrCoRuO_{6-x}H_y$ phases when heated in a sealed system and the $P(H_2)$ is allowed to rise.

The origin of the contrasting reaction pathways adopted by $LaSrCoRuO_6$ (reduce-and-exchange) and the analogous $n = 1$ Ruddlesden–Popper phase, $LaSr_3CoRuO_8$ (reduce-then-exchange)[20] is unclear. However, it should be noted that the reactivity of $LaSrCoRuO_6$ was enhanced by rapid quenching, in a manner analogous to that reported for $LaSrNiRuO_6$.[21] This quenching process could have the effect of lowering the activation barriers for both reductive anion deintercalation and anion exchange, making them more similar and resulting in the observed reactivity.

As noted above, it is clear that the hydrogen partial pressure influences the progress of hydride-for-oxide anion-exchange in the $LaSrCoRuO_{6-x}H_y$ system, and similar effects have been seen during the preparation of other oxyhydride phases. For example, the hydrogen content in $LnSrCoO_{3+x}H_y$ phases has been observed to be strongly dependent on the hydrogen pressure in the system during synthesis.[22] Similarly, the hydrogen content in $BaTiO_{3-x}H_y$ phases is also observed to be strongly dependent on the synthesis procedure used.[23-25] However, despite the obvious influence of $P(H_2)$ on the formation of oxyhydride phases, the microscopic role of H_2 gas in the formation of oxyhydride phases is not immediately clear.

While it is tempting to assume the role of the hydrogen atmosphere is to supply the hydrogen which is simply inserted into vacant oxide phases (i.e., $ABO_{3-x} + H_2 \rightarrow ABO_{3-x}H_y$), there is limited evidence for this occurring. Indeed, in many cases direct reaction of hydrogen gas with complex transition-metal oxides yields anion-deficient phases, which can only be converted to oxyhydride phases on the addition of binary metal hydrides, not further reaction with hydrogen gas alone.[18,19] Furthermore, the simple insertion of hydrogen requires the formal oxidation of the vacant oxide phase with hydrogen, which is both chemically unlikely and inconsistent with the observation of redox-neutral anion exchange processes. However, while there is little evidence for direct oxidative insertion of hydrogen, there is evidence for some interaction between hydrogen gas and oxyhydride phases, most notably in the observation of H/D exchange when D_2 is passed over $BaTiO_{3-x}H_y$ at 400 °C.[23]

Given the arguments and observations above, we propose that the role of the hydrogen atmosphere in the synthesis of transition-metal oxyhydrides is not to supply hydrogen for the anion exchange step but to stabilize the oxyhydride phases formed against hydrogen loss. Specifically, we propose that in the $LaSrCoRu(O/H)_n$ system (and the majority of other topochemically prepared transition-metal oxyhydrides), the hydride-for-oxide anion exchange reaction, which converts $LaSrCoRuO_{6-x}$ to $LaSrCoRuO_{6-2x}H_{2x}$, occurs via an all-solid-state route in which oxide and hydride ions are exchanged between $LaSrCoRuO_{6-x}$ and LiH or CaH_2 without the formation of hydrogen gas. We further propose that at the reaction temperature, the oxyhydrides formed are likely to be unstable with respect to entropy-driven H_2 loss as shown in reaction Scheme 2. We propose that the role of the H_2 gas is to

Scheme 2. Role of H_2 gas in Stabilizing Oxyhydride Phases during Synthesis

$$LaSrCoRuO_{6-x} + xCaH_2 \rightarrow LaSrCoRuO_{6-2x}H_{2x} + xCaO$$

$$\Updownarrow$$

$$LaSrCoRuO_{6-2x} + {^x\!/_2}\,H_2$$
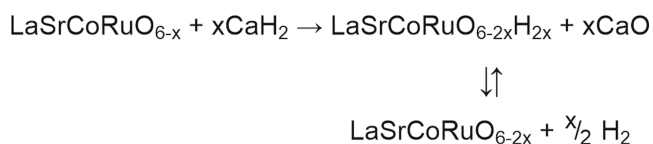
drive the resulting equilibrium towards hydrogen-rich oxyhydride phases, preventing their decomposition back to all-oxide materials. Such a scenario is consistent with the observation that $LaSrCoRuO_xH_y$ phases do not form under low $P(H_2)$ but cannot be made by the direct action of H_2 on $LaSrCoRuO_6$ in the absence of LiH or CaH_2. Further support for this scenario comes from the observed release of H_2 from sample B when heated under N_2 at 375 °C, as shown in Figure S5. While we have described the role of H_2 gas specifically in the synthesis of $LaSrCoRuO_xH_y$ phases, we think it is likely to

apply widely in the topochemical synthesis of transition-metal oxyhydrides.

Magnetism. The ferromagnetic behavior of $LaSrCoRuO_4$ is similar to that of the analogous nickel phase, $LaSrNiRuO_4$ (T_c = 250 K)[26] and the related reduced Ruddlesden–Popper oxide phases $LaSr_3NiRuO_6$ (T_c = 105 K) and $LaSr_2NiRuO_5$ (T_c = 200 K).[27] The ferromagnetic behavior of $LaSrNiRuO_6$ can be rationalized on the basis of superexchange couplings between S = 1/2 Ni^{1+} and S = 1 Ru^{2+} as shown in Figure 8.
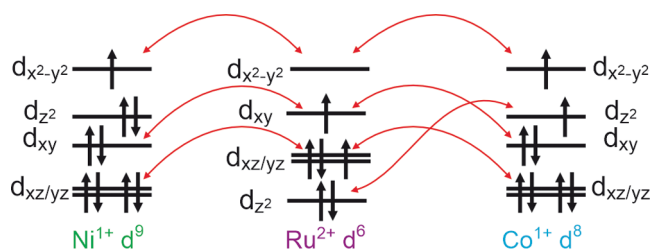

Figure 8. Superexchange interactions between square-planar Ni^{1+} or Co^{1+} and Ru^{2+}. Red arrows indicate ferromagnetic interactions.

An analogous case can be made for the ferromagnetic behavior of $LaSrCoRuO_4$. However, in this case, the d^8 electron count of Co^{1+} leads to an S = 1 configuration, which results in four ferromagnetic orbital couplings (Figure 8), compared to three in $LaSrNiRuO_4$, consistent with the higher Curie temperature for the cobalt phase (T_c > 350 K) compared to the nickel phase (T_c = 250 K).[26]

The magnetization data collected from the $LaSrCoRuO_xH_y$ phases in sample A and sample B are consistent with antiferromagnetic interactions between localized moments on Co and Ru. This behavior is hard to explain on the basis of simple superexchange interactions because when 5 or 6 coordinate, the $Co^{1+/2+}$ centers would be expected to adopt $(t_{2g})^{5/6}(e_g)^2$ configurations, which should couple to the $Ru^{2+/3+}$ $(t_{2g})^{5/6}(e_g)^0$ cations via strong ferromagnetic σ−superexchange interactions. Similar unexpected antiferromagnetic couplings are also observed between the $(t_{2g})^5(e_g)^2$ Co^{2+} and $(t_{2g})^3(e_g)^0$ Ru^{5+} centers in the parent $LaSrCoRuO_6$ oxide phase,[13] adding to the body of evidence that many $3d/4d$ transition-metal oxide system exhibit magnetic behavior that cannot be rationalized by simple superexchange couplings.

■ CONCLUSIONS

Reaction between $LaSrCoRuO_6$ and LiH or CaH_2 yields $LaSrCoRuO_xH_y$ oxyhydride phases if the $P(H_2)$ in the system is sufficient to stabilize these products with respect to hydrogen loss. Conversely, reaction between $LaSrCoRuO_6$ and LiH under low $P(H_2)$ conditions yields the infinite layer phase $LaSrCoRuO_4$, which exhibits insulating ferromagnetic behavior due to strong σ-type superexchange between Co^{1+} and Ru^{2+} centers. The influence of the local $P(H_2)$ on the competition between the formation of vacant oxides and oxyhydrides offers a method to control topochemical reductions to produce products with the desired oxide/hydride anion ratios.

■ ASSOCIATED CONTENT

Ⓢ Supporting Information

The Supporting Information is available free of charge at https://pubs.acs.org/doi/10.1021/acs.inorgchem.4c01568.

Complete structural characterization of LaSrCoRuO$_6$; thermogravimetric data from samples A, B and C; electron diffraction data from sample B; description of iodometric titration of sample A; description of the ferromagnetic subtraction method; complete magnetic characterization of sample C (PDF)

■ AUTHOR INFORMATION

Corresponding Author
Michael A. Hayward − *Department of Chemistry, University of Oxford, Inorganic Chemistry Laboratory, Oxford OX1 3QR, U.K.;* ⬤ orcid.org/0000-0002-6248-2063; Email: michael.hayward@chem.ox.ac.uk

Authors
Zhilin Liang − *Department of Chemistry, University of Oxford, Inorganic Chemistry Laboratory, Oxford OX1 3QR, U.K.*

Maria Batuk − *EMAT, University of Antwerp, Antwerp B-2020, Belgium;* ⬤ orcid.org/0000-0003-1411-9785

Fabio Orlandi − *ISIS Facility, Rutherford Appleton Laboratory, Chilton, Oxon OX11 0QX, U.K.;* ⬤ orcid.org/0000-0001-6333-521X

Pascal Manuel − *ISIS Facility, Rutherford Appleton Laboratory, Chilton, Oxon OX11 0QX, U.K.*

Joke Hadermann − *EMAT, University of Antwerp, Antwerp B-2020, Belgium;* ⬤ orcid.org/0000-0002-1756-2566

Complete contact information is available at:
https://pubs.acs.org/10.1021/acs.inorgchem.4c01568

Author Contributions
The manuscript was written through contributions of all authors

Notes
The authors declare no competing financial interest.

■ ACKNOWLEDGMENTS

■ REFERENCES

(1) Hayward, M. A. Soft chemistry synthesis of oxides. In *Comprehensive Inorganic Chemistry II*, Reedijk, J.; Poeppelmeier, K. R. Eds.; Vol. 2; Elsevier, 2013; pp 417−453.

(2) Hayward, M. A. Topochemical Reactions of Layered Transition-Metal Oxides. *Semicond. Sci. Technol.* **2014**, *29* (6), No. 064010.

(3) Hayward, M. A. Synthesis and Magnetism of Extended Solids Containing Transition-Metal Cations in Square-Planar, MO4 Coordination Sites. *Inorg. Chem.* **2019**, *58* (18), 11961−11970.

(4) Hayward, M. A.; Green, M. A.; Rosseinsky, M. J.; Sloan, J. Sodium hydride as a powerful reducing agent for topotactic oxide deintercalation: Synthesis and characterization of the nickel(I) oxide LaNiO$_2$. *J. Am. Chem. Soc.* **1999**, *121* (38), 8843−8854.

(5) Tsujimoto, Y.; Tassel, C.; Hayashi, N.; Watanabe, T.; Kageyama, H.; Yoshimura, K.; Takano, M.; Ceretti, M.; Ritter, C.; Paulus, W. Infinite-layer Iton oxide with a square-plannar coordination. *Nature* **2007**, *450*, 1062−1065.

(6) Dixon, E.; Hadermann, J.; Ramos, S.; Goodwin, A. L.; Hayward, M. A. Mn(I) in an Extended Oxide: The Synthesis and Characterization of La$_{1-}$xMnO$_{2+\delta}$ ($0.6 \leq \times \leq 1$). *J. Am. Chem. Soc.* **2011**, *133* (45), 18397−18405.

(7) Seddon, J.; Suard, E.; Hayward, M. A. Topotactic reduction of YBaCo$_2$O$_5$ and LaBaCo$_2$O$_5$: square-planer Co(I) in an extended oxide. *J. Am. Chem. Soc.* **2010**, *132*, 2802−2810.

(8) Denis Romero, F.; Burr, S. J.; McGrady, J. E.; Gianolio, D.; Cibin, G.; Hayward, M. A. SrFe$_{0.5}$Ru$_{0.5}$O$_2$: Sqaure-planar Ru^{2+} in an Extended Oxide. *J. Am. Chem. Soc.* **2013**, *135*, 1838−1844.

(9) Page, J. E.; Morgan, H. W. T.; Zeng, D.; Manuel, P.; McGrady, J. E.; Hayward, M. A. Sr$_2$FeIrO$_4$: square-planar Ir(II) in an extended oxide. *Inorg. Chem.* **2018**, *57*, 13577−13585.

(10) Hayward, M. A.; Cussen, E. J.; Claridge, J. B.; Bieringer, M.; Rosseinsky, M. J.; Kiely, C. J.; Blundell, S. J.; Marshall, I. M.; Pratt, F. L. The hydride anion in an extended transition metal oxide array: LaSrCoO$_3$H$_{0.7}$. *Science* **2002**, *295* (5561), 1882−1884.

(11) Jin, L.; Lane, M.; Zeng, D.; Kirschner, F. K. K.; Lang, F.; Manuel, P.; Blundell, S. J.; McGrady, J. E.; Hayward, M. A. LaSr$_3$NiRuO$_4$H$_4$: a 4d transition-metal oxide-hydride containing metal hydride sheets. *Angew. Chem., Int. Ed.* **2018**, *57*, 5025−5028.

(12) Kim, S. H.; Battle, P. D. Structural and electronic properties of the mixed Co Ru perovskites AA'CoRuO$_6$ (A, A' = Sr, Ba, La). *J. Solid State Chem.* **1995**, *114* (1), 174−183.

(13) Bos, J. W. G.; Attfield, J. P. Structural, magnetic, and transport properties of (La$_{1+x}$Sr$_{1-x}$)CoRuO$_6$ double perovskites. *Chem. Mater.* **2004**, *16* (9), 1822−1827.

(14) Coelho, A. A. TOPAS and TOPAS-Academic: an optimization program integrating computer algebra and crystallographic objects written in C plus. *J. Appl. Crystallogr.* **2018**, *51*, 210−218.

(15) Liang, Z.; Batuk, M.; Orlandi, F.; Manuel, P.; Hadermann, J.; Hayward, M. A. Disproportionation of Co^{2+} in the Topochemically Reduced Oxide LaSrCoRuO$_5$. *Angew. Chem.* **2024**, *63*, No. e202313067.

(16) Adkin, J. J.; Hayward, M. A. Room temperature antiferromagnetic order in the Mn(II) oxide 4H-Ba$_{0.5}$Sr$_{0.5}$MnO$_{2+d}$. *Inorg. Chem.* **2008**, *47*, 10959−10964.

(17) Denis Romero, F.; Leach, A.; Müller, J. S.; Foronda, F.; Blundell, S.; Hayward, M. A. Strontium Vanadium Oxide−Hydrides: "Square-Planar" Two-Electron Phases. *Angew. Chem., Int. Ed.* **2014**, *53*, 7556−7559.

(18) Bridges, C. A.; Darling, G. R.; Hayward, M. A.; Rosseinsky, M. J. Electronic strcutre, magnetic ordering and formation pathway of the transition metal oxide hydride LaSrMnO$_3$H$_{0.7}$. *J. Am. Chem. Soc.* **2005**, *127*, 5996−6011.

(19) Hayward, M. A.; Rosseinsky, M. J. Anion vacancy distribution and magnetism in the new reduced layers Co(II)/Co(I) phase LaSrCoO$_{3.5-x}$. *Chem. Mater.* **2000**, *12*, 2182−2195.

(20) Jin, L.; Batuk, M.; Kirschner, F. K. K.; Lang, F.; Blundell, S. J.; Hadermann, J.; Hayward, M. A. Exsolution of SrO during the Topochemical Conversion of LaSr$_3$CoRuO$_8$ to the Oxyhydride LaSr$_3$CoRuO$_4$H$_4$. *Inorg. Chem.* **2019**, *58* (21), 14863−14870.

(21) Liang, Z.; Amano Patino, M.; Hendrickx, M.; Hadermann, J.; Hayward, M. A. Microstructural Activation of a Topochemical Reduction Reaction. *ACS Org. Inorg. Au* **2022**, *2*, 75−82.

(22) Bowman, A.; Claridge, J. B.; Rosseinsky, M. J. Anion composition control and magnetic short and long range order in transition metal oxide-hydrides. *Chem. Mater.* **2006**, *18*, 3046−3056.

(23) Kobayashi, Y.; Hernandez, O. J.; Sakaguchi, T.; Yajima, T.; Roisnel, T.; Tsujimoto, Y.; Morita, M.; Noda, Y.; Mogami, Y.; Kitada, A.; et al. An oxyhydride of BaTiO$_3$ exhibiting hydride exchange and electronic conductivity. *Nat. Mater.* **2012**, *11* (6), 507−511.

(24) Bouilly, G.; Yajima, T.; Terashima, T.; Yoshimune, W.; Nakano, K.; Tassel, C.; Kususe, Y.; Fujita, K.; Tanaka, K.; Yamamoto, T.; et al. Electrical Properties of Epitaxial Thin Films of Oxyhydrides ATiO(3-x)H(x) (A = Ba and Sr). *Chem. Mater.* **2015**, *27* (18), 6354−6359.

(25) Nedumkandathil, R.; Jaworski, A.; Grins, J.; Bernin, D.; Karlsson, M.; Eklöf-Österberg, C.; Neagu, A.; Tai, C.-W.; Pell, A. J.;

Häussermann, U. Hydride Reduction of BaTiO3 − Oxyhydride Versus O Vacancy Formation. *Acs Omega* **2018**, *3* (9), 11426−11438.

(26) Amano Patino, M.; Zeng, D.; Bower, R.; McGrady, J. E.; Hayward, M. A. Coupled electronic and magnetic phase transition in the infinite-layer phase LaSrNiRuO₄. *Inorg. Chem.* **2016**, *55* (17), 9012−9016.

(27) Xu, Z. Y.; Jin, L.; Backhaus, J. K.; Green, F.; Hayward, M. A. Hole and Electron Doping of Topochemically Reduced Ni(I)/Ru(II) Insulating Ferromagnetic Oxides. *Inorg. Chem.* **2021**, *60* (19), 14904−14912.